RSC Advances

COMMUNICATION

View Article Online
View Journal | View Issue

Cite this: *RSC Adv.*, 2015, **5**, 34088

Received 22nd February 2015
Accepted 23rd March 2015

DOI: 10.1039/c5ra03308j

www.rsc.org/advances

Amorphous titanate-crosslinking N-rich carbon hybrid with 3D channels for fast lithium storage†

Jiehua Liu,*[a] Jiaqi Xu,[a] Kuan Zhou,[a] Lei Wang[b] and Xiangfeng Wei[ac]

Carbon-based anodes are considered as the preferred choice owing to their unique properties, but they are limited by poor high-rate performance and capacities. To overcome the volume swell of layered materials like graphite, a novel amorphous titanate-crosslinking N-rich carbon hybrid is successfully prepared for the first time using a facile one-pot method. Due to the stable 3D framework with a good distribution of nitrogen and titanium, the obtained hybrid demonstrates a high reversible capacity of 523.3 mA h g^{-1} at the high rate of 2 A g^{-1}, much higher than the theoretical value (372 mA h g^{-1}) of layered graphite. This hybrid anode also exhibits superior high-rate capability and cycling performance, possibly serving as a novel sustainable material for lithium-ion batteries and supercapacitors.

Introduction

The carbon-based anode is considered as the preferred choice for next-generation lithium-ion batteries (LIBs) because of its structural, thermal and electronic properties.[1–3] Compared to the rapid development of cathodes, high-performance anode materials are still urgently needed.[4–6] The lithium-storage performance of the anode is one of the most important factors contributing to a higher energy density, power density and a shortened charging time. To meet market requirements, lithium capacity, rate performance and cost are the three major considerations in the context of advanced LIBs with carbon-based anode materials. For example, carbon nanotubes with a 1D structure are limited in wider applications due to high costs and small scale production.[7,8] Graphite, as one of the important carbon materials with 2D channels, has been widely employed in commercial LIBs due to its high theoretical capacity of 372 mA h g^{-1}, but it often exhibits poor cycling performance and low capacity at high rates because of the structural swell limitation.[9,10]

Nitrogen-rich 1D or 2D carbon materials also exhibit improved capacities for lithium storage, but the high costs of these hybrid carbon-based materials and the complex processes restrict their extensive applications.[11,12] Titanium based anode materials exhibit stable structures that contribute to an excellent performance for fast lithium storage, such as sandwich-like titanate nanosheets[13,14] and lithium titanate.[15,16] However, their relatively-low capacities and anode potential make them less competitive for LIBs. To overcome these shortcomings, titanate–carbon composites were fabricated with improved performances from a synergistic effect.[17,18] However, most of the titanates employed in the composites are crystalline structures, which still limit the overall capacities of the composites. An amorphous composite might have unexpected results for lithium storage, but few results, if any, have appeared about amorphous titanate–carbon hybrids in the literature. We have a great interest in creating new ways to fabricate these new structures.

We noticed that graphitic C_3N_4 (g-C_3N_4) not only has a similar two dimensional nano-architecture to graphite (Scheme 1a), but also exhibits distinctive semiconductor properties.[19–24] However, g-C_3N_4 is often overlooked in the field of energy storage due to its low capacity for lithium storage. The synthesis process of g-C_3N_4 is easier and gentler than that of graphite. Also, substrates (*e.g.* melamine, urea) with amino groups provide huge potential for developing functional carbon-based materials. To overcome the volume swell of layered materials, crosslinking agents may be employed to improve their stability performance as shown in Scheme 1b. After *in situ* carbonization, 3D channels will be formed *in situ* (Scheme 1c). The obtained titanate-crosslinking N-rich carbon

[a]*Future Energy Laboratory, School of Materials Science and Engineering, Hefei University of Technology, Tunxi Road No. 193, Hefei, Anhui, 230009, China. E-mail: liujh@hfut.edu.cn*

[b]*Department of Chemistry and Biochemistry, University of South Carolina, Columbia, SC 29208, USA*

[c]*School of Chemical Engineering, Hefei University of Technology, Tunxi Road No. 193, Hefei, Anhui, 230009, China*

† Electronic supplementary information (ESI) available: Experimental details, FTIR spectra, XRD curve, XPS spectrum and cyclic voltammetry curves. See DOI: 10.1039/c5ra03308j

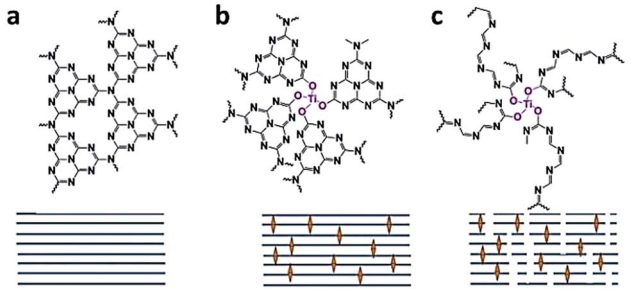

Scheme 1 (a) g-C_3N_4 with 2D channels; (b) titanate crosslinking g-C_3N_4 hybrid with 2D channels; (c) N-rich carbon–titanate hybrid with 3D channels.

hybrid (TNCH) with 3D channels may be an alternative host for lithium storage. In this work, the possibility of higher lithium storage capacity was explored by an *in situ* one-pot method of fabrication. According to this process, the amorphous material, consisting of carbon, nitrogen and titanate, offers 3D channels for fast Li^+ intercalation. The amorphous hybrid exhibits higher capacities and better rate performance than individual graphite or titanate, and is particularly applicable to fast lithium storage.

Results and discussion

Fig. 1a and b show TEM images of the TNCH. Fig. 1a shows an irregular morphology of grains. Fig. 1b provides direct evidence

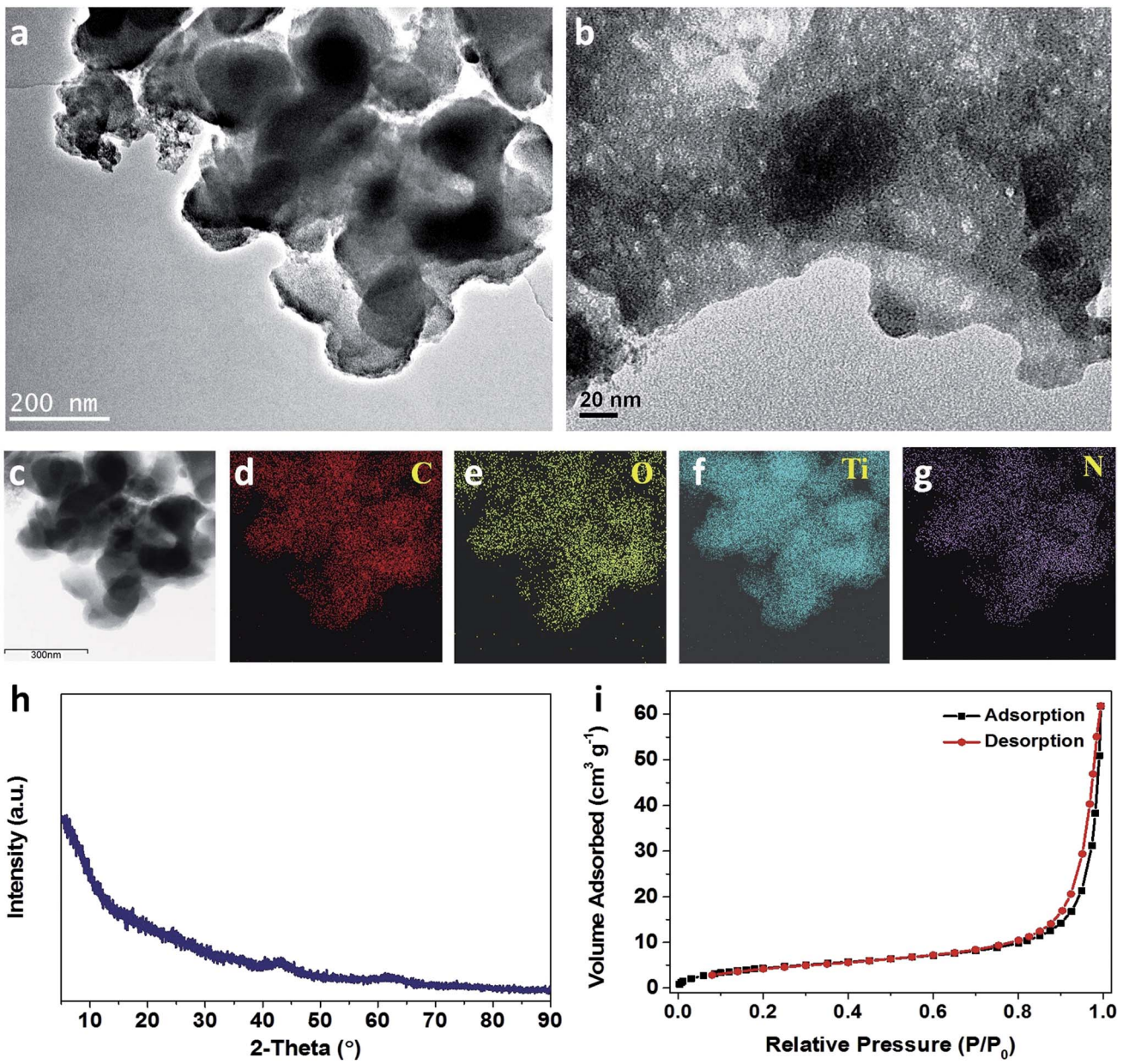

Fig. 1 (a) and (b) TEM images; (c)–(g) STEM images, C, O, Ti and N mappings, respectively; (h) XRD pattern and (i) N_2 adsorption–desorption isotherms of TNCH.

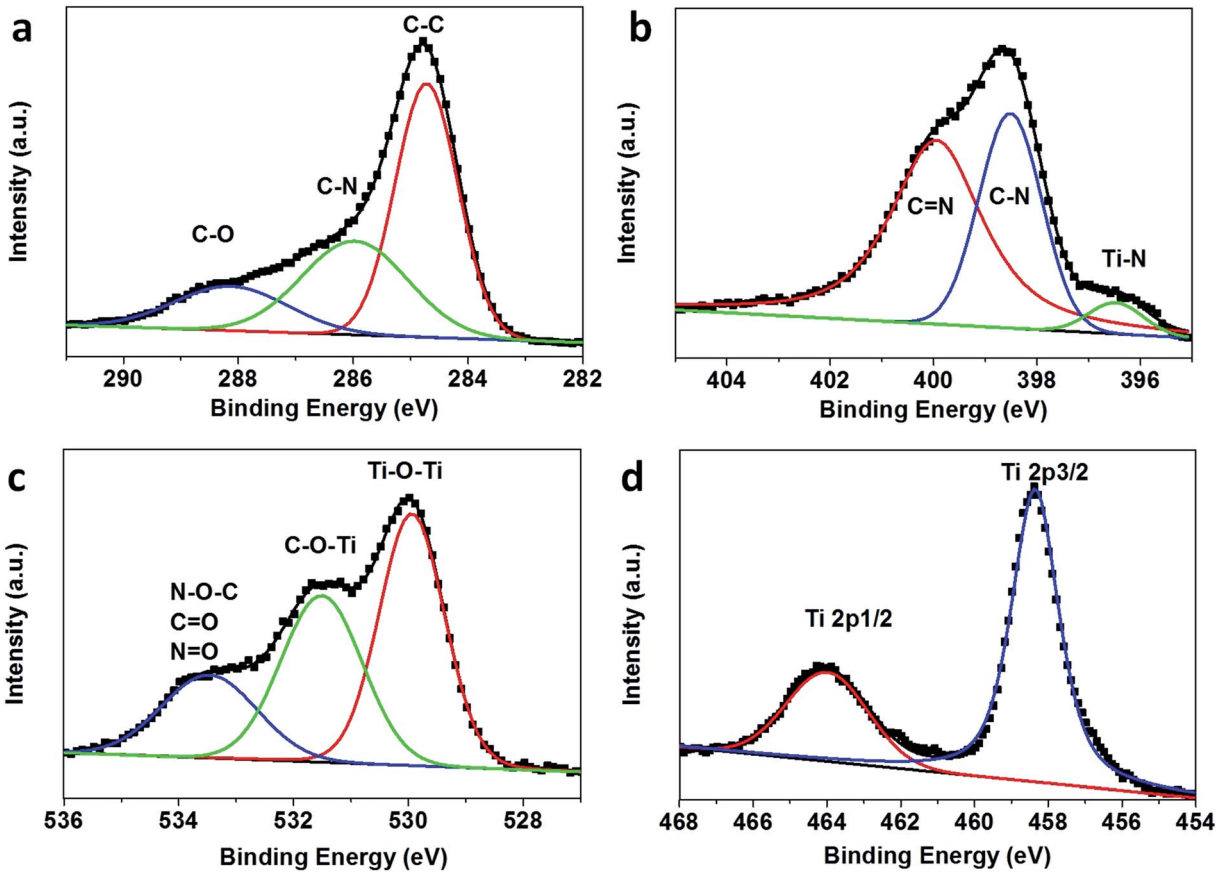

Fig. 2 High resolution XPS spectra of (a) C 1s, (b) N 1s, (c) O 1s and (d) Ti 2p in the TNCH.

of the proposed 3D structure, clearly showing nanoporous 3D channels. Fig. S1† shows HRTEM and fast Fourier transform images of the enlarged outer surface in Fig. 1a, which is a typical amorphous structure with a disordered atomic structure. To further confirm the formation of 3D channels, Fig. S2† shows TEM images of intermediates which were annealed at 500 °C for 2 hours (Fig. S2a†) and 650 °C for 1 hour (Fig. S2b†). There are obvious 3D channels obtained at 650 °C rather than at 500 °C. The STEM image (Fig. 1c) and the corresponding elemental mappings (Fig. 1d–g) of C, O, Ti and N revealed that C, O, Ti and N were evenly distributed in the TNCH grains. In Fig. 1h, no strong characteristic peak of TNCH was detected in the XRD pattern, which reveals an amorphous structure and excludes the existence of crystalline TiO_2, graphite and g-C_3N_4 (Fig. S3†),[25] which supports our proposal in Scheme 1c. A little amount cubic of titanium oxide (JCPDS card no. 89-3660) or titanium nitride (JCPDS card no. 87-0627) may be obtained in the reducing atmospheres which were produced by the decomposition of C_3N_4. As shown in Fig. 1i, the BET specific surface area of TNCH is 16.8 $m^2\ g^{-1}$ and the total pore volume of 0.096 $cm^3\ g^{-1}$ was concluded using adsorption data.

Fig. S4† shows the Fourier-transform infrared (FT-IR) spectra of g-C_3N_4 and TNCH, which exhibit the presence of polymeric N-heterocycles. The overall spectral features of g-C_3N_4 obtained at 650 °C without the Ti crosslinking agent are similar to those of the reported g-C_3N_4.[26,27] The absorption bands centered at 1574 and 1637 cm^{-1} are attributed to C=N stretching, while the multiple bands between 1200 and 1500 cm^{-1} to aromatic C–N stretching. A broad band at 2900–3400 cm^{-1} belongs to the stretching modes of $-NH_2$ or =NH groups which is in agreement with the results from the XPS analysis (Fig. S5†). In particular, all of the above characteristic absorption peaks in g-C_3N_4 nearly disappear in the spectrum of TNCHs, indicating that the g-C_3N_4 structure was destroyed in the reaction with titanate.

XPS measurements were employed to define the chemical environment of the elements based on their binding energy and to determine the main components of the TNCH. A full XPS spectrum detected the signals for C 1s, N 1s, O 1s and Ti 2p in the near surface range of the TNCH (Fig. S5†). The atomic percentages of C, N, O and Ti are 56.67%, 14.79%, 21.73% and 6.83%, respectively. It is worth noting that the ratio of O and Ti in the sample is 3.18 : 1, much higher than the ratio in TiO_2. It is possible that the melamine reacted with titanic acid to form a new and stable Ti–O–C bond *via* deamination. These results further prove that the role of titanate is the crosslinking agent.

High-resolution XPS spectra are provided in Fig. 2. The C 1s XPS spectrum shows an asymmetrical peak, and the deconvoluted core level spectrum with peaks at 284.72, 285.98 and 288.38 eV has been presented in Fig. 2a. The major peak at 284.72 eV is exclusively assigned to carbon atoms (C–C bonding) in a pure carbon environment, *i.e.*, amorphous carbon in our

sample or adsorbed to the surface.[28] The peaks at 285.98 and 288.38 eV are ascribed to the existence of C–O/C–N and C=O/C=N bonds respectively.[29] The N 1s XPS spectrum (Fig. 2b) indicates the co-existence of a number of distinguishable N environments corresponding to three peaks at binding energies of 396.48, 398.52 and 399.95 eV. The two peaks at 398.86 and 399.95 eV can be assigned to N atoms in a C=N–C microenvironment and tertiary nitrogens, respectively.[30,31] The peak at 396.48 eV may be attributed to Ti–N, implying that the conductivity could be improved in the hybrid. In Fig. 2c, the curve fitting of the O 1s spectrum basically indicates three components centered at 529.94, 531.52 and 533.50 eV in the TNCH, which are attributed to Ti–O–Ti, Ti–O–C and C=O respectively.[29,32] As indicated in Fig. 2d, the binding energies of Ti $2p_{3/2}$ and $2p_{1/2}$ are centered at 458.36 and 464.00 eV, in agreement with those of Ti^{4+} in TiO_2.[33]

The electrochemical studies of the TNCH were performed using coin cells with Li metal slices serving as both the counter and reference electrodes at room temperature. More details are provided in the experimental section in the ESI.† The cyclic voltammetric curve (Fig. S6†) of the electrode made of TNCH was performed at a scanning rate of 0.2 mV s^{-1}. The typical current curves are obvious with a voltage range of 0.01 V and 3 V, which show that the insertion–deinsertion mechanism is very similar to graphene-based materials. The peak in the 2nd cycle is lower than that in the 1st cycle and confirms the formation of a solid–electrolyte interface film.

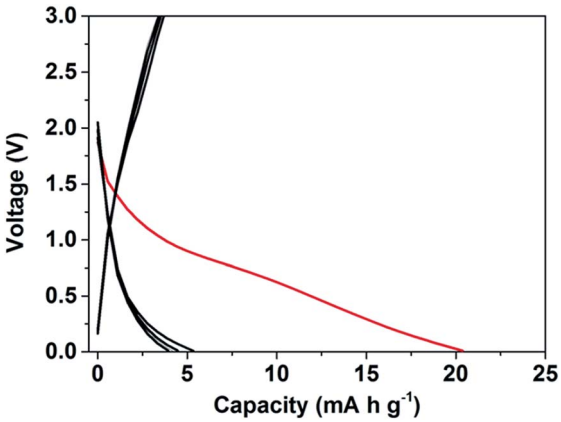

Fig. 4 Charge–discharge profiles of g-C_3N_4 obtained without the titanate crosslinking agent at a rate of 0.1 A g^{-1}.

Fig. 3a shows the first two charge–discharge voltage profiles for the TNCH at a current density of 2.0 A g^{-1} between a voltage of 0.05 V and 3.00 V. These results demonstrate that the TNCH has the typical discharge–charge characteristics of amorphous

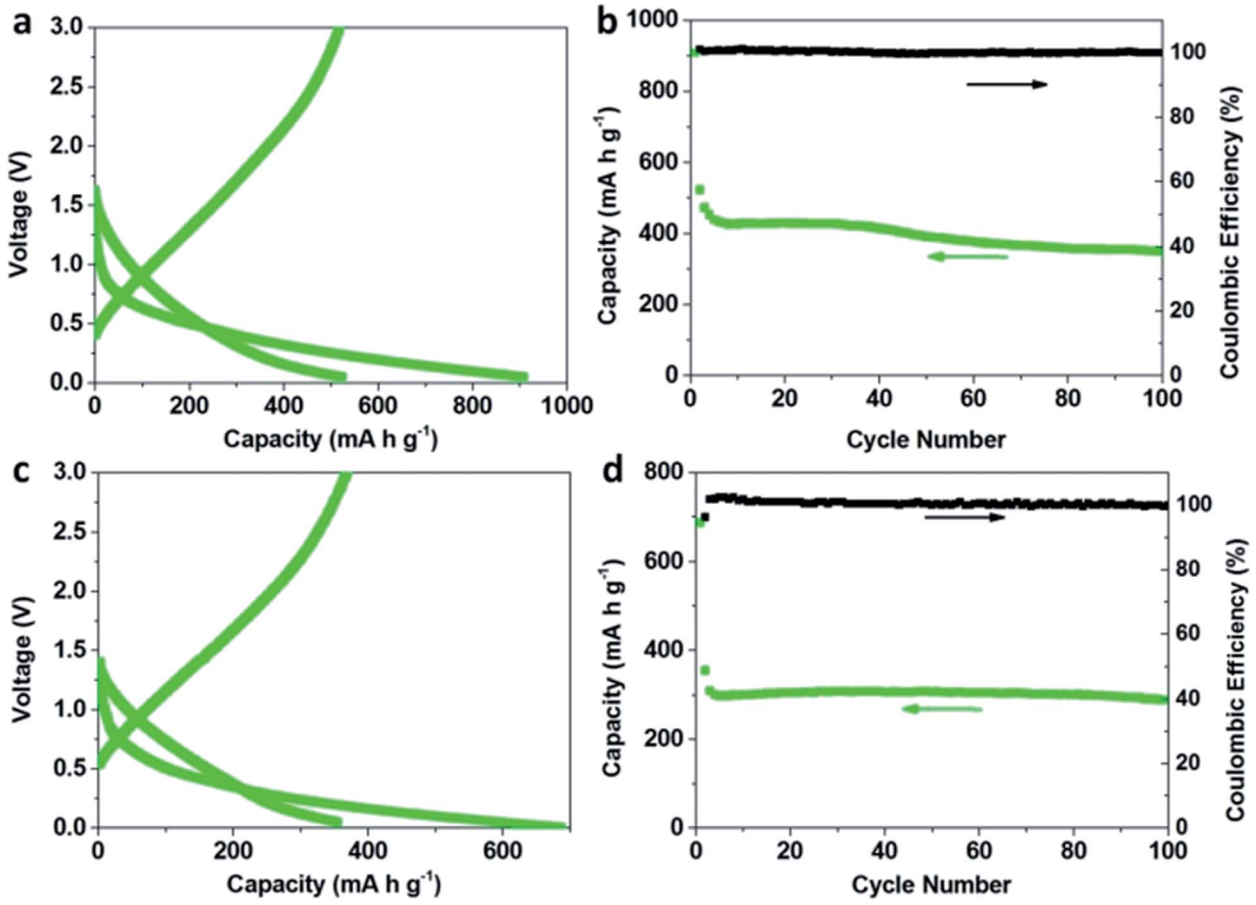

Fig. 3 Charge–discharge profiles, reversible capacities and the Coulombic efficiency of the TNCH at high rates of 2.0 A g^{-1} (a and b) and 5.0 A g^{-1} (c and d) respectively.

carbon. The TNCH delivered a first-discharge capacity of 908.8 mA h g^{-1} and charge capacity of 518.3 mA h g^{-1}. The reversible capacity of the TNCH anode at the second cycle is about 523.3 mA h g^{-1}, revealing a high Coulombic efficiency of 101%. Fig. 3b shows that the Coulombic efficiency is maintained at nearly 100% at the second and the sequential cycles, which indicates that the formed interface is stable during cycling. After the 40th cycle, the discharge capacity of TNCH remains 414.4 mA h g^{-1}, which is higher than the theoretical capacity (372 mA h g^{-1}) of graphite. After the 100th cycle, the discharge capacity of the TNCH is kept at 351.1 mA h g^{-1}.

A current density of 5.0 A g^{-1} was set to further investigate the higher rate performance of the TNCH. In Fig. 3c, the first-discharge capacity is 687.8 mA h g^{-1} with discharge cut-off voltages of 0.01 V in consideration of the polarization potential at the higher rate. The cut-off voltage range of 0.05–3 V is used in sequential cycles for comparing with the performance at 2 A g^{-1}. The discharge capacity of the TNCH at the second cycle is 355 mA h g^{-1} with a Coulombic efficiency of 96.2% because of the higher discharge cut-off voltage of 0.05 V. Fig. 3d indicates that the discharge capacity and Coulombic efficiency of the TNCH is maintained at 288.4 mA h g^{-1} and ~100%, respectively, after the 100th cycle, much better than some reported examples of amorphous carbon and graphite.[34]

Comparative experiments were conducted to investigate the capacity of the material obtained in the absence of Ti^{4+} as the crosslinking agent. The structure of the typical g-C_3N_4 sample obtained by annealing at 650 °C for 2 hours has been confirmed by XRD analysis in Fig. S3.† The g-C_3N_4 sample gives very low capacities compared to the sample with Ti^{4+}, as shown in Fig. 4. The first discharge capacity is only 20.3 mA h g^{-1} and less than 4 mA h g^{-1} is retained after 5 cycles. Therefore, we conclude that Ti^{4+} not only plays an important role in the formation of stable TNCHs, but also reacts with g-C_3N_4 to form a N-rich carbon hybrid with 3D channels.

The excellent electrochemical performance of TNCH is probably rooted in its stable nano-architecture with the following features: (1) titanate plays a propping role and improves the framework of the TNCH which possesses 3D channels for lithium transport. (2) The existence of Ti–N bonding also enhances the conductivity of anode. (3) The usage of titanic acid can enhance the yield of g-C_3N_4 and TNCH to lower the cost. Therefore, the desired material could be applied into batteries or supercapacitors owing to the superior performance for fast lithium storage.

Conclusions

In summary, we synthesized an amorphous N-rich titanate–carbon hybrid using a one-pot solid state reaction with step-by-step heat treatments including polymerization and followed by *in situ* carbonization at 500 and 650 °C, respectively. The amorphous Ti-stable and N-rich framework provides stable 3D channels for lithium-ion transport. Moreover, electrochemical measurements demonstrate that this hybrid can deliver a reversible capacity of 523.3 mA h g^{-1} at the high rate of 2.0 A g^{-1}, much higher than theoretical value of graphite. Therefore, this hybrid anode also exhibits superior high-rate capability and cycling performance. The reported method provides a new pathway to develop low cost and sustainable materials for fast lithium storage.

Acknowledgements

This research was supported by the Natural Science Foundation of China (21303038), a Heifei University of Technology start-up grant (407037069), and the Hundred Talents Program of Anhui Province.

Notes and references

1 C. N. R. Rao, K. Gopalakrishnan and A. Govindaraj, *Nano Today*, 2014, **9**, 324–343.
2 I. V. Lightcap and P. V. Kamat, *Acc. Chem. Res.*, 2013, **46**, 2235–2243.
3 A. D. Roberts, X. Li and H. F. Zhang, *Chem. Soc. Rev.*, 2014, **43**, 4341–4356.
4 P. Barpanda, M. Ati, B. C. Melot, G. Rousse, J. N. Chotard, M. L. Doublet, M. T. Sougrati, S. A. Corr, J. C. Jumas and J. M. Tarascon, *Nat. Mater.*, 2011, **10**, 772–779.
5 H. G. Zhang, X. D. Yu and P. V. Braun, *Nat. Nanotechnol.*, 2011, **6**, 277–281.
6 H. Liu, F. C. Strobridge, O. J. Borkiewicz, K. M. Wiaderek, K. W. Chapman, P. J. Chupas and C. P. Grey, *Science*, 2014, 344.
7 Z. Y. Cao and B. Q. Wei, *Energy Environ. Sci.*, 2013, **6**, 3183–3201.
8 Q. Zhang, J. Q. Huang, W. Z. Qian, Y. Y. Zhang and F. Wei, *Small*, 2013, **9**, 1237–1265.
9 H. Ota, Y. Sakata, A. Inoue and S. Yamaguchi, *J. Electrochem. Soc.*, 2004, **151**, A1659–A1669.
10 M. Lu, H. Cheng and Y. Yang, *Electrochim. Acta*, 2008, **53**, 3539–3546.
11 L. G. Bulusheva, A. V. Okotrub, A. G. Kurenya, H. K. Zhang, H. J. Zhang, X. H. Chen and H. H. Song, *Carbon*, 2011, **49**, 4013–4023.
12 K. N. Wood, R. O'Hayre and S. Pylypenko, *Energy Environ. Sci.*, 2014, **7**, 1212–1249.
13 J. H. Liu, J. S. Chen, X. F. Wei, X. W. Lou and X. W. Liu, *Adv. Mater.*, 2011, **23**, 998–1002.
14 J. H. Liu and X. W. Liu, *Adv. Mater.*, 2012, **24**, 4097–4111.
15 G. N. Zhu, Y. G. Wang and Y. Y. Xia, *Energy Environ. Sci.*, 2012, **5**, 6652–6667.
16 Y. Sun, L. Zhao, H. L. Pan, X. Lu, L. Gu, Y. S. Hu, H. Li, M. Armand, Y. Ikuhara, L. Q. Chen and X. J. Huang, *Nat. Commun.*, 2013, **4**, 1870.
17 Y. G. Guo, J. S. Hu and L. J. Wan, *Adv. Mater.*, 2008, **20**, 2878–2887.
18 D. H. Wang, D. W. Choi, J. Li, Z. G. Yang, Z. M. Nie, R. Kou, D. H. Hu, C. M. Wang, L. V. Saraf, J. G. Zhang, I. A. Aksay and J. Liu, *ACS Nano*, 2009, **3**, 907–914.
19 J. Liang, Y. Zheng, J. Chen, J. Liu, D. Hulicova-Jurcakova, M. Jaroniec and S. Z. Qiao, *Angew. Chem., Int. Ed.*, 2012, **51**, 3892–3896.

20 G. Liu, P. Niu, C. H. Sun, S. C. Smith, Z. G. Chen, G. Q. Lu and H. M. Cheng, *J. Am. Chem. Soc.*, 2010, **132**, 11642–11648.
21 X. D. Zhang, X. Xie, H. Wang, J. J. Zhang, B. C. Pan and Y. Xie, *J. Am. Chem. Soc.*, 2013, **135**, 18–21.
22 P. Niu, L. C. Yin, Y. Q. Yang, G. Liu and H. M. Cheng, *Adv. Mater.*, 2014, **26**, 8046–8052.
23 D. J. Martin, K. P. Qiu, S. A. Shevlin, A. D. Handoko, X. W. Chen, Z. X. Guo and J. W. Tang, *Angew. Chem., Int. Ed.*, 2014, **53**, 9240–9245.
24 G. H. Dong, Z. H. Ai and L. Z. Zhang, *RSC Adv.*, 2014, **4**, 5553–5560.
25 S. Kumar, T. Surendar, B. Kumar, A. Baruah and V. Shanker, *RSC Adv.*, 2014, **4**, 8132–8137.
26 F. He, G. Chen, Y. G. Yu, Y. S. Zhou, Y. Zheng and S. Hao, *Chem. Commun.*, 2015, **51**, 425–427.
27 J. H. Li, B. A. Shen, Z. H. Hong, B. Z. Lin, B. F. Gao and Y. L. Chen, *Chem. Commun.*, 2012, **48**, 12017–12019.
28 K. Dai, L. H. Lu, C. H. Liang, Q. Liu and G. P. Zhu, *Appl. Catal., B*, 2014, **156**, 331–340.
29 J. Yu, G. Dai, Q. Xiang and M. Jaroniec, *J. Mater. Chem.*, 2011, **21**, 1049–1057.
30 S. W. Bian, Z. Ma and W. G. Song, *J. Phys. Chem. C*, 2009, **113**, 8668–8672.
31 L. Ge and C. C. Han, *Appl. Catal., B*, 2012, **117**, 268–274.
32 J. G. Yu, H. G. Yu, B. Cheng, X. J. Zhao, J. C. Yu and W. K. Ho, *J. Phys. Chem. B*, 2003, **107**, 13871–13879.
33 J. Wang, C. Fan, Z. Ren, X. Fu, G. Qian and Z. Wang, *Dalton Trans.*, 2014, **43**, 13783–13791.
34 Y. Fang, Y. Y. Lv, R. C. Che, H. Y. Wu, X. H. Zhang, D. Gu, G. F. Zheng and D. Y. Zhao, *J. Am. Chem. Soc.*, 2013, **135**, 1524–1530.